レーザー顕微鏡の解像限界算出のためのダイアグラム法

福武直樹*

Diagram method for resolution limit calculation in laser microscopy

Naoki FUKUTAKE*

顕微鏡の光学分解能は，「光の回折に起因した限界がある」とよく表現される．アッベにより，この回折限界という特性が示され，明視野顕微鏡の結像理論の基礎となった．アッベの結像理論が定式化された当時は，照明された試料からの透過光を用いて像を形成する技術しかなかったが，現在は蛍光を含む様々な光学現象が顕微鏡に使われている．蛍光には回折という概念が存在しないため，当初の顕微鏡には機能していた回折限界の原理は，蛍光顕微鏡には適用できない．実際，蛍光共焦点顕微鏡は回折限界を超えた光学分解能を示す．にもかかわらず，初期の回折限界が未だすべての顕微鏡の評価基準となっていることは驚きに値する．様々な光学現象を用いた顕微鏡の解像限界を比較するために，統一結像理論を構築することは有益である．我々は，量子光学的結像理論を定式化し，そこから光学現象ごとに解像限界が定義されることを導出した．この理論は，アッベの理論を最低次の光学現象を用いるケースとして含み，さらにすべての高次の光学現象を一つの統一式によって表現している．我々は，すべての光学現象をファインマンダイアグラムで描き，ダイアグラムから解像限界を計算する手法を導いた．

In this work, we study the influence of optical processes on the resolution limit of laser microscopes. We formulate rules of resolution limit calculation for all types of laser microscopes that employ a variety of optical processes occurring in a sample. By replacing the field with creation/annihilation operators, we develop a theoretical framework to unify image-forming formulas that cover all interactions between molecules in the sample and the light excitation including the vacuum field. To determine some simple rules for the evaluation of optical resolution, our theoretical framework provides a diagram method that describes linear, nonlinear, coherent, and incoherent optical processes. According to our formulas, the type of optical process decisively influences the resolution limit if no *a priori* information on the sample exists.

Key words 結像理論，解像限界，顕微鏡，光と物質の相互作用，ファインマンダイアグラム
image-forming theory, resolution limit, microscopy, double-sided Feynman diagram, optical process

1 Introduction

In 1873, Ernst Abbe established the modern theory of image formation in optical microscopy and derived the well-known formula for the optical resolution, $d = \lambda/2NA$, which corresponds to a frequency cutoff (resolution limit) of $2NA/\lambda$, where λ is the wavelength of light and NA is the numerical aperture of microscope objective[1]. In fact, classical microscopies, such as bright field microscopy[2], phase contrast microscopy[3)4)], differential interference microscopy[5], and dark field microscopy[6] essentially follow Abbe's theorem. Relatively new microscopy modalities, such as relief contrast microscopy[7], digital holographic microscopy[8], and optical coherence tomography[9] also obey Abbe's rule.

Recently, laser microscopy systems based on a variety of optical processes have been developed[10)~14)]. Although Abbe's definition of resolution limit is still used as the standard, it is relatively unknown that the $2NA/\lambda$-limit can be applied only to microscopies based on electric susceptibility $\chi^{(1)}$-derived optical processes, such as linear absorption (LA), transmission, and reflection. Furthermore, considering the three dimensional (3-D) optical resolution in transmission microscopy, it is known that the missing cone exists in the spatial-frequency domain[15], as long as the $\chi^{(1)}$-derived optical processes are used. When using higher order nonlinear susceptibility $\chi^{(i)}$-derived optical processes ($i \geq 2$), the reso-

* 研究開発本部　光技術研究所

lution limit may surpass $2NA/\lambda$ and the missing cone can be overcome[16]. This implies that the higher order optical processes, even fluorescence, which is a $\chi^{(3)}$-derived optical process, cannot be dealt with by Abbe's formula. Indeed, the frequency cutoff in fluorescence confocal microscopy is $4NA/\lambda$[15].

In this study, we formulated the rules for the resolution limit calculation of all laser microscopes that employ arbitrary optical processes. In our theory, the resolution limit can be calculated by using the double-sided Feynman diagrams describing the time evolution of the density matrix. In nonlinear optics, the Feynman diagram method was originally developed for the classification of optical processes and the calculation of $\chi^{(i)}$ [17]. We extended the applicability of the diagram method to the calculation of the resolution limit. Our theory covers the Abbe's formula as a special case of the lowest order $\chi^{(1)}$ optical process. Linear, nonlinear, coherent, and incoherent optical processes can all be described by the diagram that includes some arrows[18]. We show that each arrow corresponds to the 3-D pupil function, following the rule we derived. The transfer function, which we will define as "3-D aperture", can be calculated by connecting all 3-D pupil functions in the diagram with convolutions. According to our theory, without *a priori* information on the sample, the type of optical process involved determines the resolution limit.

2 Optical process: Feynman diagram description

Many types of optical processes can be employed for optical microscopy, as shown in Fig. 1(a). All optical processes, including coherent and incoherent ones, can be described by double-sided Feynman diagrams[17][18]. As an example, Fig. 1(b) shows the diagrams describing linear fluorescence (FL). In general, optical processes are expressed by simultaneous plural diagrams. For example, in FL, three diagrams exist that contribute to the optical process[18]. In an incoherent process such as FL, both the vacuum field and the laser beam are involved. Because solid arrows are generally used to represent the excitation field (real photons) in a diagram, we use a dotted arrow to represent the vacuum field. A left-pointing wavy arrow emerging from the ket side (left side) corresponds to the signal field.

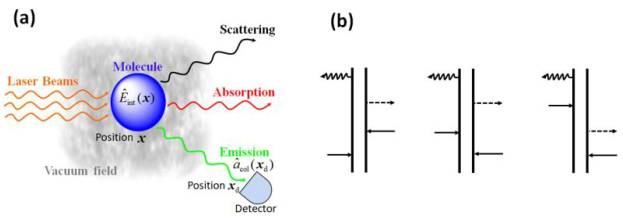

Fig. 1 (a) Schematic of light-matter interaction. (b) Examples of Feynman diagrams (three diagrams for FL)

In this section, we analyze the fundamental mathematics underlying the physical phenomena by using the quantum-optical notation to deal with all optical processes, including incoherent processes. Before dealing with microscopy, we analyze the simple case where the creation and annihilation of the excitation photons occur in free space with the transition of molecules (including virtual transition), which results in the creation of a signal photon from the molecule and its annihilation at the detection position (see Fig. 1(a)). In a diagram, left- and right-pointing arrows correspond to creation operators $\hat{a}^{+}(\boldsymbol{x})$ and annihilation operators $\hat{a}(\boldsymbol{x})$, respectively, where $\boldsymbol{x} = (x, y, z)$. We establish the drawing rule of the wavy arrow for the signal field, in which the arrow for the signal invariably emerges from the ket side to avoid the redundant addition of diagrams. The wavy arrow corresponds to $\hat{a}^{+}_{\mathrm{sig}}(\boldsymbol{x})$ (see Appendix). We define the interaction operator $\hat{E}_{\mathrm{int}}(\boldsymbol{x})$ as the product of all operators in the diagram of interest and the excitation operator $\hat{E}_{\mathrm{ex}}(\boldsymbol{x})$, i.e., $\hat{E}_{\mathrm{int}}(\boldsymbol{x}) = \hat{E}_{\mathrm{ex}}(\boldsymbol{x})\,\hat{a}^{+}_{\mathrm{sig}}(\boldsymbol{x})$. The excitation operator for the i-th order optical process is composed of i creation/annihilation operators.

Some typical diagrams are shown in Fig. 2, where the optical processes are categorized in terms of the order i. Although some optical processes are depicted by simultaneous plural diagrams, one of them is described as a representative diagram for each optical process. Note that the diagrams representing identical optical processes indicate the same optical resolution. The inner dotted line indicates the longitudinal relaxation, which does not influence the optical resolution. In incoherent optical processes, the vacuum field is involved as a local oscillator and one of the excitation fields, while in coherent optical processes only the laser beams are responsible for the excitation. In coherent optical

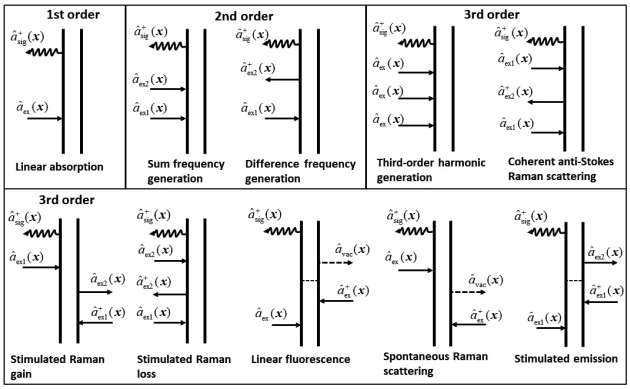

Fig. 2 Typical diagrams for some optical processes

processes, the presence of the local oscillator depends on the type of optical process.

3 Notation system

First, we consider the phenomenon in free space. Fig. 1(a) represents a laser beam incident on a molecular ensemble with nonlinear susceptibility $\chi^{(i)}$, where the light-matter interaction occurs. Then, the molecular ensemble radiates the signal, which propagates to the detector position $\boldsymbol{x}_\mathrm{d}$, where it is annihilated. We assume the laser beam to be in coherent state $|\alpha\rangle$. We also incorporate the vacuum state around the sample $|0\rangle$ into the formulation (see Appendix). Under the excitation condition $|\alpha\rangle|0\rangle$, the expectation value of the signal created at $\boldsymbol{x}$ and detected at $\boldsymbol{x}_\mathrm{d}$ can be expressed as $\langle 0|\langle\alpha|\chi^{(i)}\hat{E}_{\mathrm{int}}(\boldsymbol{x})\hat{a}(\boldsymbol{x}_\mathrm{d})|\alpha\rangle|0\rangle$. For example, in LA, by using the equation $\hat{E}_{\mathrm{int}}(\boldsymbol{x}) = \hat{a}_\alpha(\boldsymbol{x})\hat{a}_0^+(\boldsymbol{x})$ with $\hat{a}_\alpha(\boldsymbol{x})$ acting on $|\alpha\rangle$ and $\hat{a}_0^+(\boldsymbol{x})$ acting on $|0\rangle$, the normalizations $\langle\alpha|\alpha\rangle = 1$ and $\langle 0|0\rangle = 1$, and the ordering rule of operators defined in Appendix (symbol $\vdots\ \vdots$), the expectation value mentioned above becomes

$$\begin{aligned}&\langle 0|\langle\alpha|\vdots\chi^{(1)}\hat{a}_\alpha(\boldsymbol{x})\hat{a}_0(\boldsymbol{x}_\mathrm{d})\hat{a}_0^+(\boldsymbol{x})\vdots|\alpha\rangle|0\rangle\\ &=\chi^{(1)}\langle\alpha|\hat{a}_\alpha(\boldsymbol{x})|\alpha\rangle\langle 0|\hat{a}_0(\boldsymbol{x}_\mathrm{d})\hat{a}_0^+(\boldsymbol{x})|0\rangle\\ &=\chi^{(1)}\alpha(\boldsymbol{x})G(\boldsymbol{x}_\mathrm{d}-\boldsymbol{x}),\end{aligned}\tag{1}$$

where $G(\boldsymbol{x}_\mathrm{d}-\boldsymbol{x})$ denotes the Green's function for the signal photon propagating from $\boldsymbol{x}$ to $\boldsymbol{x}_\mathrm{d}$ and $\alpha(\boldsymbol{x})$ is the complex function obtained from the equation $\hat{a}_\alpha(\boldsymbol{x})|\alpha\rangle = \alpha(\boldsymbol{x})|\alpha\rangle$. In Eq. (1), we used suffixes α for the laser and 0 for the vacuum to clarify the state that the operator acts on. In free space without lenses, although $\hat{a}_0(\boldsymbol{x})$ still corresponds to $\hat{a}_{\mathrm{sig}}(\boldsymbol{x})$, $\hat{a}_0(\boldsymbol{x}_\mathrm{d})$ is not equal to $\hat{a}_{\mathrm{col}}(\boldsymbol{x}_\mathrm{d})$:

$$\hat{a}_0^+(\boldsymbol{x}) = \hat{a}_{\mathrm{sig}}^+(\boldsymbol{x})\tag{2}$$

$$\hat{a}_0(\boldsymbol{x}_\mathrm{d}) = \int\hat{a}(\boldsymbol{f}_\mathrm{d})e^{i2\pi\boldsymbol{f}_\mathrm{d}\cdot\boldsymbol{x}_\mathrm{d}}d^3\boldsymbol{f}_\mathrm{d}.\tag{3}$$

Considering the interaction between the signal field described by Eq. (1), which is generated from the vacuum field, and the excitation laser beam itself, which acts as a local oscillator, the expectation value of the intensity observed by the detector at $\boldsymbol{x}_\mathrm{d}$ is given by

$$\begin{aligned}&\langle 0|\langle\alpha|\vdots\left|-i\hat{a}_\alpha(\boldsymbol{x}_\mathrm{d})+\chi^{(1)}\hat{E}_{\mathrm{int}}(\boldsymbol{x})\hat{a}_0(\boldsymbol{x}_\mathrm{d})\right|^2\vdots|\alpha\rangle|0\rangle\\ &\approx\langle 0|\langle\alpha|\Big\{\hat{a}_\alpha^+(\boldsymbol{x}_\mathrm{d})\hat{a}_\alpha(\boldsymbol{x}_\mathrm{d})\\ &\quad+i\chi^{(1)}\hat{a}_\alpha^+(\boldsymbol{x}_\mathrm{d})\hat{a}_\alpha(\boldsymbol{x})\hat{a}_0(\boldsymbol{x}_\mathrm{d})\hat{a}_0^+(\boldsymbol{x}_\mathrm{d})+h.c.\Big\}|\alpha\rangle|0\rangle\\ &=\left|\alpha(\boldsymbol{x}_\mathrm{d})\right|^2+i\chi^{(1)}\alpha^*(\boldsymbol{x}_\mathrm{d})\alpha(\boldsymbol{x})G(\boldsymbol{x}_\mathrm{d}-\boldsymbol{x})+c.c.\end{aligned}\tag{4}$$

where the fourth term was neglected and the Gouy phase shift $-i$ added in the vicinity of the focus of the local oscillator was considered.

4 Microscopy model description

We now define the imaging system (laser microscopy) in our model. The laser microscopy is composed of an excitation system that focuses the laser beam onto a sample and a signal-collection system that gathers the signal generated from the sample. A schematic of laser microscopy with the coordinate system is shown in Fig. 3. In the following, we assume a 3-D sample-stage scanning, rather than laser scanning, which, however, does not influence the optical resolution. In laser microscopy, one or two excitation beams are usually employed to generate the signal. The electric field of the signal is emitted from the molecule excited by the electric fields of the excitation beams, and the signal field propagates through the signal-collection system. The signals are acquired point by point with a photodetector to reconstruct the 3-D image.

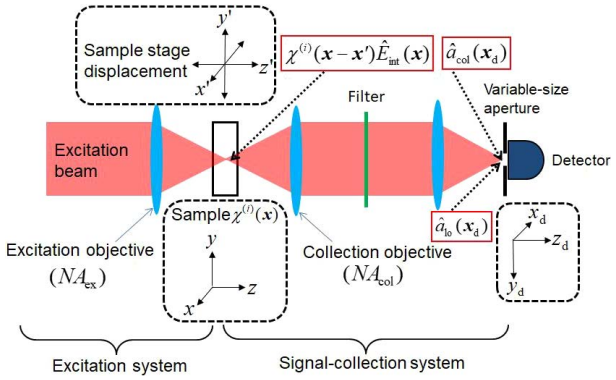

Fig. 3 Schematic of laser microscopy with coordinate systems

For simplicity, the first Born approximation is applied to understand the true nature of the optical resolution. In this approximation, multiple scattering and depletion of the beam are neglected, which usually holds true for nearly transparent samples, such as biological specimens. If multiple scattering and depletion are intense, the image acquired will be deformed to some extent. We assume that both the excitation and signal-collection systems are 1-X magnification systems, which does not change the essence of the image-forming properties. In our model, the scalar diffraction theory is employed. The linear or nonlinear susceptibility distribution $\chi^{(i)}(x, y, z)$ in the sample acts as an object in the imaging system. The excitation electric field induces the polarization, which emits the signal electric field.

5 Quantum image-forming theory

The interaction operator $\hat{E}_{\mathrm{int}}(\boldsymbol{x})$ is the product of all operators in the diagram of interest corresponding to the excita-

tion fields (laser, vacuum, etc.) and the signal field. In Appendix, the creation $\hat{a}^{+}(\boldsymbol{x})$ and annihilation $\hat{a}(\boldsymbol{x})$ operators for the excitation and signal fields in real space, respectively, are found from the inverse Fourier transform of the product of the 3-D pupil function, $P(\boldsymbol{f})$, and the operators in wavenumber space, $\hat{a}^{+}(\boldsymbol{f})$ or $\hat{a}(\boldsymbol{f})$. When the sample-stage displacement $\boldsymbol{x}' = (x', y', z')$ is zero, the operator for the polarization distribution in the sample formed by the excitation objective is expressed by $\chi^{(i)}\,\hat{E}_{\mathrm{ex}}(\boldsymbol{x})$, where we presume that the electric permittivity ε_0 is unity: $\varepsilon_0 = 1$. As mentioned above, $\hat{E}_{\mathrm{ex}}(\boldsymbol{x})$ is the operator composed of the product of the operators in the diagram of interest except for $\hat{a}^{+}_{\mathrm{sig}}(\boldsymbol{x})$. The expectation value of the amplitude of the signal generated at $\boldsymbol{x}$ in the sample and detected at $\boldsymbol{x}_{\mathrm{d}}$ is represented by

$$\begin{aligned}&\langle 0|_{\mathrm{ex}}\langle\alpha|\chi^{(1)}\vdots\widehat{E}_{\mathrm{int}}(\boldsymbol{x})\hat{a}_{\mathrm{col}}(\boldsymbol{x}_{\mathrm{d}})\vdots|\alpha\rangle_{\mathrm{ex}}|0\rangle\\ &=\langle 0|_{\mathrm{ex}}\langle\alpha|\chi^{(1)}\vdots\widehat{E}_{\mathrm{ex}}(\boldsymbol{x})\vdots\hat{a}_{\mathrm{col}}(\boldsymbol{x}_{\mathrm{d}})\hat{a}^{+}_{\mathrm{sig}}(\boldsymbol{x})|\alpha\rangle_{\mathrm{ex}}|0\rangle,\end{aligned}\tag{5}$$

where all operators appearing in the diagram and $\hat{a}_{\mathrm{col}}(\boldsymbol{x}_{\mathrm{d}})$ are defined in Appendix; the excitation state $|\alpha\rangle_{\mathrm{ex}}$ is also defined in Appendix. The signal emitted from a single point $\boldsymbol{x}$ in the sample forms the electric field distribution, i.e., the amplitude spread function (*ASF*), at the detection position $\boldsymbol{x}_{\mathrm{d}}$:

$$ASF_{\mathrm{col}}(\boldsymbol{x}_{\mathrm{d}}-\boldsymbol{x})=\langle 0|\hat{a}_{\mathrm{col}}(\boldsymbol{x}_{\mathrm{d}})\hat{a}^{+}_{\mathrm{sig}}(\boldsymbol{x})|0\rangle.\tag{6}$$

Integrating Eq. (5) over the object space, the total amplitude of the signal at $\boldsymbol{x}_{\mathrm{d}}$ becomes

$$\langle 0|_{\mathrm{ex}}\langle\alpha|\iiint\chi^{(1)}(\boldsymbol{x})\vdots\widehat{E}_{\mathrm{int}}(\boldsymbol{x})\hat{a}_{\mathrm{col}}(\boldsymbol{x}_{\mathrm{d}})\vdots d^3x|\alpha\rangle_{\mathrm{ex}}|0\rangle.\tag{7}$$

In addition to the signal, we need to consider the local oscillator forming the electric-field distribution in the detecting space. For coherent optical processes, one of the excitation laser beams becomes the local oscillator that forms the electric field distribution through the excitation and signal-collection systems. For incoherent optical processes, the vacuum field around the sample acts as a local oscillator reaching the detecting space through the signal-collection system. Considering the interaction between the signal field and the local oscillator, the intensity observed at the detecting point $\boldsymbol{x}_{\mathrm{d}}$ is given by

$$\langle 0|_{\mathrm{ex}}\langle\alpha|\vdots\left|-i\hat{a}_{\mathrm{lo}}(\boldsymbol{x}_{\mathrm{d}})+\iiint\chi^{(i)}(\boldsymbol{x})\widehat{E}_{\mathrm{int}}(\boldsymbol{x})\hat{a}_{\mathrm{col}}(\boldsymbol{x}_{\mathrm{d}})d^3x\right|^2\vdots|\alpha\rangle_{\mathrm{ex}}|0\rangle,\tag{8}$$

where the operator for the local oscillator $\hat{a}_{\mathrm{lo}}(\boldsymbol{x}_{\mathrm{d}})$ is introduced and the Gouy phase shift of $-i$ for the local oscillator is considered. The operator $\hat{a}_{\mathrm{lo}}(\boldsymbol{x}_{\mathrm{d}})$ becomes $\hat{a}_{\mathrm{lo(I)}}(\boldsymbol{x}_{\mathrm{d}})$ acting on $|\alpha\rangle_{\mathrm{ex}}$ or $\hat{a}_{\mathrm{lo(v)}}(\boldsymbol{x}_{\mathrm{d}})$ acting on $|0\rangle$ depending on the optical process. Note that, while some of the coherent optical processes are not involved in the local oscillator, which is the vacuum field, in this case, the contribution of the local oscillator inevitably vanishes because of the formulas $\hat{a}_{\mathrm{lo(v)}}(\boldsymbol{x}_{\mathrm{d}})|0\rangle = 0$ and $\langle 0|\hat{a}^{+}_{\mathrm{lo(v)}}(\boldsymbol{x}_{\mathrm{d}}) = 0$.

Taking into account the sample-stage displacement $\boldsymbol{x}'$, we rewrite Eq. (8) as

$$\langle 0|_{\mathrm{ex}}\langle\alpha|\vdots\left|-i\hat{a}_{\mathrm{lo}}(\boldsymbol{x}_{\mathrm{d}})+\iiint\chi^{(i)}(\boldsymbol{x}-\boldsymbol{x}')\widehat{E}_{\mathrm{int}}(\boldsymbol{x})\hat{a}_{\mathrm{col}}(\boldsymbol{x}_{\mathrm{d}})d^3x\right|^2\vdots|\alpha\rangle_{\mathrm{ex}}|0\rangle.\tag{9}$$

To discuss the resolution limit, we consider confocal microscopy, which has the largest frequency cutoff derived from a specific optical process. The image intensity acquired by confocal microscopes can be expressed as

$$I(\boldsymbol{x}')=\langle 0|_{\mathrm{ex}}\langle\alpha|\vdots\left|-i\hat{a}_{\mathrm{lo}}(\boldsymbol{0})+\iiint\chi^{(i)}(\boldsymbol{x}-\boldsymbol{x}')\widehat{E}_{\mathrm{int}}(\boldsymbol{x})\hat{a}_{\mathrm{col}}(\boldsymbol{0})d^3x\right|^2\vdots|\alpha\rangle_{\mathrm{ex}}|0\rangle,\tag{10}$$

where $\boldsymbol{0}$ means $\boldsymbol{x}_{\mathrm{d}} = (0, 0, 0)$, indicating the detection position.

6 Image-forming formulas for each optical process

We give some examples of the image-forming formulas for confocal microscopy with a variety of optical processes. We start with Eq. (10) for all optical processes, including linear, nonlinear, coherent, and incoherent ones.

(1) Coherent optical process

In coherent optical processes, the presence of local oscillators depends on the optical process. For example, in LA, stimulated Raman gain (SRG), stimulated Raman loss (SRL), and stimulated emission (SE), the local oscillator and signal interfere at the detecting position. By contrast, in sum frequency generation (SFG), difference frequency generation (DFG), and third-order harmonic generation (THG), the signal does not interfere with the excitation laser beam because the latter can be blocked with a filter by using the wavelength difference. In coherent anti-Stokes Raman scattering (CARS), two signals, namely the CARS and four wave mixing (often referred to as non-resonant back ground), interfere, causing the non-resonant background to act as a local oscillator.

For coherent optical processes with local oscillators, Eq. (10) becomes

$$\begin{aligned}I_{\mathrm{C(lo)}}(\boldsymbol{x}')=&\left|\alpha_{\mathrm{lo(I)}}h_{\mathrm{lo(I)}}(\boldsymbol{0})\right|^2\\&+i\alpha^{*}_{\mathrm{lo(I)}}h^{*}_{\mathrm{lo(I)}}(\boldsymbol{0})\iiint\chi^{(i)}(\boldsymbol{x}-\boldsymbol{x}')E_{\mathrm{ex}}(\boldsymbol{x})h_{\mathrm{col}}(-\boldsymbol{x})d^3x\\&+c.c.,\end{aligned}\tag{11}$$

where the equations $\langle 0|\ \hat{a}_{\mathrm{col}}(\boldsymbol{0})\ \hat{a}^{+}_{\mathrm{sig}}\ (\boldsymbol{x})\,|0\rangle = ASF_{\mathrm{col}}\ (-\boldsymbol{x}) \equiv h_{\mathrm{col}}(-\boldsymbol{x})$, $\hat{a}_{\mathrm{lo}(1)}(\boldsymbol{0})\,|\alpha\rangle_{\mathrm{ex}} = \alpha_{\mathrm{lo}(1)}\ h_{\mathrm{lo}(1)}\ (\boldsymbol{0})\,|\alpha\rangle_{\mathrm{ex}}$, ${}_{\mathrm{ex}}\langle\alpha|\alpha\rangle_{\mathrm{ex}} = 1$, and $\langle 0|0\rangle = 1$ were considered and the fourth term was neglected; the scalar function $E_{\mathrm{ex}}(\boldsymbol{x}) = {}_{\mathrm{ex}}\langle\alpha|\ \vdots\ \hat{E}_{\mathrm{ex}}(\boldsymbol{x})\ \vdots\ |\alpha\rangle_{\mathrm{ex}}$ indicates the product of i ASFs formed by the excitation beams. The ASF of the collection system $ASF_{\mathrm{col}}\ (\boldsymbol{x}) \equiv h_{\mathrm{col}}\ (\boldsymbol{x})$ includes information on the signal wavelength and the *NA* of the signal-collection system. Note that $ASF_{\mathrm{lo(l)}}\ (\boldsymbol{0}) \equiv h_{\mathrm{lo(l)}}\ (\boldsymbol{0})$ includes the contributions of the *NA* of both the excitation and collection systems and the excitation wavelength. Because the first term in Eq. (11) is a constant, the second term determines the resolution limit. We refer to the function $E_{\mathrm{ex}}(\boldsymbol{x})\ h_{\mathrm{col}}(-\boldsymbol{x}) \equiv h_{\mathrm{t}}(-\boldsymbol{x})$ as the ASF of the total microscope system and its Fourier transform corresponds to the 3-D aperture. In this case, the 3-D aperture is often referred to as the weak-object transfer function (WOTF)[19]. The complex constants α_{ex1}, α_{ex2}, etc. correspond to the laser power amplitude, and $h_{\mathrm{ex1}}\ (\boldsymbol{x})$, $h_{\mathrm{ex2}}\ (\boldsymbol{x})$, etc. include the information on the excitation wavelength and the *NA* of the excitation system.

For coherent optical processes without local oscillators, Eq. (10) becomes

$$I_{\mathrm{C}}(\boldsymbol{x}') = \left|\iiint \chi^{(i)}(\boldsymbol{x}-\boldsymbol{x}')E_{\mathrm{ex}}(\boldsymbol{x})h_{\mathrm{col}}(-\boldsymbol{x})d^3\boldsymbol{x}\right|^2, \tag{12}$$

where the first term $\langle 0|\hat{a}_{\mathrm{lo(v)}}(\boldsymbol{0})\ \hat{a}^{+}_{\mathrm{lo(v)}}\ (\boldsymbol{x})\,|0\rangle$, which cannot be observed, was neglected; the second and third terms vanish because the numbers of the creation and annihilation operators acting on $|0\rangle$ are different, and only the fourth term remains. In Eq. (12), we use the equation $\hat{a}_{\mathrm{col}}\ (\boldsymbol{0})\ \hat{a}^{+}_{\mathrm{col}}\ (\boldsymbol{0}) = \hat{a}^{+}_{\mathrm{col}}\ (\boldsymbol{0})\ \hat{a}_{\mathrm{col}}\ (\boldsymbol{0}) + C$ (const.) originating from the commutation relation $[\hat{a}_{\mathrm{col}}\ (\boldsymbol{0}),\ \hat{a}^{+}_{\mathrm{col}}\ (\boldsymbol{0})] = \int |P_{\mathrm{col}}\ (\boldsymbol{f}_{\mathrm{d}})|^2\ d^3\ \boldsymbol{f}_{\mathrm{d}}$ (see Appendix), which results in the part $C\langle 0|\hat{a}_{\mathrm{sig}}(\boldsymbol{x}_2)\ \hat{a}^{+}_{\mathrm{sig}}\ (\boldsymbol{x}_1)\,|0\rangle$ vanishing because the Green's function $\langle 0|\ \hat{a}_{\mathrm{sig}}(\boldsymbol{x}_2)\ \hat{a}^{+}_{\mathrm{sig}}\ (\boldsymbol{x}_1)\,|0\rangle$ propagating from $\boldsymbol{x}_1$ to $\boldsymbol{x}_2$ is not related to the physical phenomenon. We also use the relation $|0\rangle\langle 0| = 1$. As mentioned above, the ASF of the total system, ASF_{T}, is represented by $h_{\mathrm{t}}(-\boldsymbol{x}) \equiv E_{\mathrm{ex}}(\boldsymbol{x})\ h_{\mathrm{col}}(-\boldsymbol{x})$. Note that grating objects with grating pitch finer than the ASF_{T} cannot be resolved by microscopes using coherent optical processes without local oscillators. Consequently, the ASF_{T} is well-defined indicator of the resolution limit.

(2) Incoherent optical process

In incoherent optical processes such as FL, two-photon excited fluorescence (TPEF), and spontaneous Raman scattering (Ra), the annihilation operator for the vacuum field emerging from the bra side in the diagram $\hat{a}_{\mathrm{vac}}(\boldsymbol{x})$ (see Appendix) is essential for $\hat{E}_{\mathrm{ex}}(\boldsymbol{x})$. In incoherent processes, the vacuum field acts as the local oscillator. We define the operator $\hat{E}_{\mathrm{ex(l)}}(\boldsymbol{x})$ as the product of all operators in the diagram excluding $\hat{a}_{\mathrm{vac}}(\boldsymbol{x})$, i.e., $\hat{E}_{\mathrm{ex}}(\boldsymbol{x}) = \hat{E}_{\mathrm{ex(l)}}(\boldsymbol{x})\ \hat{a}_{\mathrm{vac}}(\boldsymbol{x})$. For an incoherent optical process, Eq. (10) reduces to the well-known image-forming formula:

$$I_{\mathrm{IC}}(\boldsymbol{x}') = \langle 0|\hat{a}_{\mathrm{lo(v)}}(\boldsymbol{0})\hat{a}^{+}_{\mathrm{lo(v)}}(\boldsymbol{x})|0\rangle - 2\iiint \mathrm{Im}\left\{\chi^{(i)}(\boldsymbol{x}-\boldsymbol{x}')\right\}|ASF_{\mathrm{ex(l)}}(\boldsymbol{x})|^2\,|h_{\mathrm{col}}(-\boldsymbol{x})|^2\,d^3\boldsymbol{x}. \tag{13}$$

In Eq. (13), the scalar function $E_{\mathrm{ex}}(\boldsymbol{x}) = {}_{\mathrm{ex}}\langle\alpha|\ \vdots\ \hat{E}_{\mathrm{ex(l)}}(\boldsymbol{x})\ \vdots\ |\alpha\rangle_{\mathrm{ex}}$ is introduced; the relation $E_{\mathrm{ex(l)}}(\boldsymbol{x}) = |ASF_{\mathrm{ex(l)}}(\boldsymbol{x})|^2$ is used because $\hat{E}_{\mathrm{ex(l)}}(\boldsymbol{x})$ is inevitably composed of the same number of $\hat{a}_{\mathrm{ex}}(\boldsymbol{x})$ and $\hat{a}^{+}_{\mathrm{ex}}\ (\boldsymbol{x})$ in incoherent optical processes; and the commutation relation $[\hat{a}_{\mathrm{col}}(\boldsymbol{0}),\ \hat{a}^{+}_{\mathrm{lo(v)}}\ (\boldsymbol{0})] = \int V^{*}(\boldsymbol{f}_{\mathrm{d}})|P_{\mathrm{col}}\ (\boldsymbol{f}_{\mathrm{d}})|^2\ d^3\ \boldsymbol{f}_{\mathrm{d}} = 0$ (see Appendix) and the formula $|0\rangle\langle 0| = 1$ are utilized. Note that $\mathrm{Im}\{\chi^{(i)}(\boldsymbol{x})\}$ is a negative function. Because the vacuum field is never observed, the first term can be omitted. The point spread function of the total system involving an incoherent optical process is $|ASF_{\mathrm{ex(l)}}(\boldsymbol{x})|^2|h_{\mathrm{col}}(-\boldsymbol{x})|^2 \equiv h_{\mathrm{t}}(-\boldsymbol{x})$.

7 Redefinition of the resolution limit

In our theory, all optical processes, including linear, nonlinear, coherent, and incoherent ones, can be dealt with considering the same framework. For coherent processes, only the real field is applied as the excitation field, while for incoherent processes, one of the excitation fields is the vacuum field.

To evaluate the resolution limit of all microscopy modalities, we define the 3-D aperture $A(\boldsymbol{f})$ as the Fourier transform of the ASF of the total system ASF_{T} represented by $h_{\mathrm{t}}(-\boldsymbol{x})$. The physical significance of the 3-D aperture is the rate of Fourier components in the object, acquired through the microscope system. In microscopy with a local oscillator, the 3-D aperture is derived from the Fourier transform of the second term (one of the cross terms) of Eq. (10), as $\widetilde{\chi^{(i)}}\ (\boldsymbol{f})A(\boldsymbol{f})$; in this case, the Fourier transform of the third term is merely the complex conjugate of the Fourier transform of the second term, which means that the third term does not contain additional information. In microscopy without local oscillators, only the fourth term remains, and its Fourier transform is proportional to the autocorrelation of $\widetilde{\chi^{(i)}}(\boldsymbol{f})A(\boldsymbol{f})$. Furthermore, because no local oscillator is present, the optical transfer function (OTF) cannot be defined, resulting in some image deformation. Because the spatial frequency outside the 3-D aperture can never be acquired, the 3-D aperture itself is the most appropriate criteria to obtain the resolution limit.

While for incoherent processes the OTF can always be defined, for coherent processes, it can be defined only if the local oscillator exists. However, the 3-D aperture can be

defined even in the absence of a local oscillator. For microscopy with the local oscillator, two types of the OTFs are defined, i.e., ones for the real and imaginary parts of $\chi^{(i)}(\boldsymbol{x})$. By taking into account the second and third terms in Eq. (10), the OTF for the real part of $\chi^{(i)}(\boldsymbol{x})$ becomes $OTF_{\mathrm{r}}(\boldsymbol{f}) = iA(\boldsymbol{f}) - iA^{*}(-\boldsymbol{f})$. Similarly, the OTF for the imaginary part can be expressed as $OTF_{\mathrm{i}}(\boldsymbol{f}) = -A(\boldsymbol{f}) - A^{*}(-\boldsymbol{f})$[19]. Although $\chi^{(i)}(\boldsymbol{x})$ is generally a complex function, in most cases $\chi^{(i)}(\boldsymbol{x})$ is either the real function or the pure imaginary function. In this case, $OTF_{\mathrm{r}}(\boldsymbol{f})$ and $OTF_{\mathrm{i}}(\boldsymbol{f})$ become well-defined and useful concepts. However, even when the OTF is not defined, the 3-D aperture is still the best indicator for the resolution limit, because the information outside the 3-D aperture cannot be acquired.

8 Rules of diagram method

As described above, in all optical processes, including incoherent and coherent, regardless of the presence or absence of the local oscillator, the 3-D aperture can be expressed by the Fourier transform of $h_{\mathrm{t}}(-\boldsymbol{x})$. The expressions for the coherent and incoherent optical processes can be unified using the diagram method. From the Fourier transform, we obtain the rule that the 3-D aperture of confocal microscopy with a certain optical process can be calculated by convolving all 3-D pupil functions that correspond to the arrows in the diagram, following the correspondence table below[20)21)]. Note that, in the table, we rewrite $P_{\mathrm{col}}(\boldsymbol{f})\,\delta_{+}^{*}(|\boldsymbol{f}|-\boldsymbol{f}_{\mathrm{sig}})$ as $P_{\mathrm{col}}(\boldsymbol{f})$, which has delta-function characteristic in the radial direction.

Table 1 Correspondence between pupil functions and the arrows in the diagrams

	Excitation	Excitation	Vacuum	Signal
arrow	⟶	⟵	⇢	⇜
Pupil function	$P_{\mathrm{ex}}(-\boldsymbol{f})$	$P_{\mathrm{ex}}^{*}(\boldsymbol{f})$	$P_{\mathrm{col}}^{*}(-\boldsymbol{f})$	$P_{\mathrm{col}}(\boldsymbol{f})$

All optical processes can be described by the diagrams, which were originally developed to classify and count the right amount of interactions and estimate the amplitude and phase of the nonlinear susceptibility in the interaction of interest. We discovered one more application of the diagrams, i.e., calculating the 3-D aperture of microscopes that employ the optical process described by the diagram, where each arrow corresponds to a 3-D pupil function: the 3-D aperture can be computed by connecting all 3-D pupil functions in a diagram with convolution. The frequency cutoff of the 3-D aperture defined above determines the resolution limit of the microscope. As long as the optical process of interest is employed, the resolution limit cannot surpass the frequency cutoff determined by the optical process, regardless of how well the system is devised. We can prove the following theorem: "If there is no *a priori* information on an object in far-field microscopy, the resolution limit determined by optical process cannot be surpassed, no matter how well the microscopy is devised."

9 Results and discussion

As stated above, the maximum possible resolution limit is determined by the type of optical process employed. For illustration, Fig. 4 shows the calculation results of the 3-D aperture for CARS, SRL, SRG, and THG microscopy[20)21)]. With identical excitation wavelengths, the resolution limits of SRL and SRG microscopy are the same, while that of CARS microscopy is higher. The 3-D aperture of THG microscopy exhibits peculiar properties, whereby the value of the origin in the spatial frequency domain is zero, resulting in the disappearance of the uniform part from the image.

According to our theory, the upper limit of the frequency cutoff determined by the optical process cannot be surpassed. Although the optical resolution may be different for different microscopy modalities, the maximal frequency cutoff is the same if the same optical process is employed. The modality with the maximal frequency cutoff is confocal microscopy. The frequency cutoff of its 3-D aperture deter-

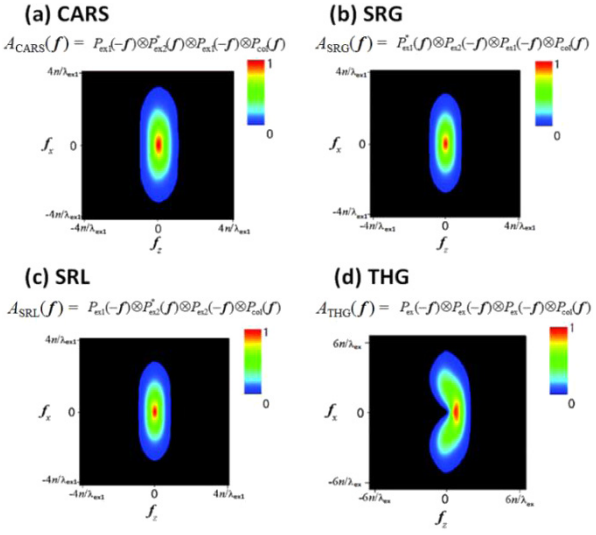

Fig. 4 Calculated 3-D apertures for (a) CARS, (b) SRG, (c) SRL, and (d) THG. n is the average refractive index in the sample. The NAs of both excitation and signal-collection objectives are 0.9 (dry). For CARS, SRG, and SRL, the vibrational frequency ($1/\lambda_{\mathrm{ex1}}-1/\lambda_{\mathrm{ex2}}$) is assumed to be 2850 cm^{-1}.

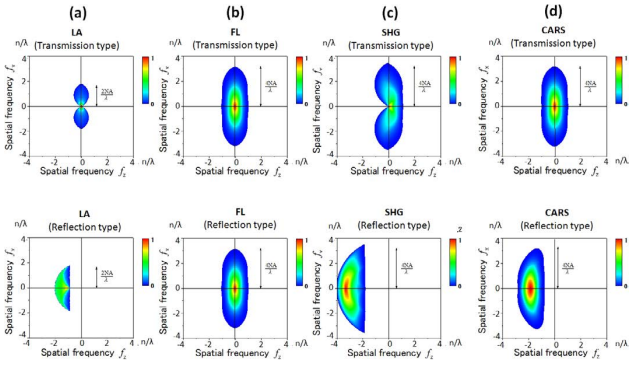

Fig. 5 Calculated 3-D apertures for (a) LA, (b) FL, (c) SHG, and (d) CARS. The upper and lower rows are for transmission and reflection types, respectively.

mines the upper limit by the optical process of interest. While each optical process possesses its own inherent upper limit, the NA and wavelength also influence the resolution. Only spatial frequencies within the 3-D aperture can be imaged. Fig. 5 shows the calculated 3-D apertures of confocal microscopy in transmission and reflection modes employing LA, FL, second-order harmonic generation (SHG), and CARS. In reflection mode, although the OTF does not exist (no local oscillator), the 3-D aperture can be defined. In Fig. 5, the NAs of both excitation and signal-collection objectives are assumed to be 1.2 (water immersion), and λ (800 nm) represents the excitation wavelength. In CARS, where two excitation beams (pump and Stokes) are used, we assume that λ is the pump wavelength (800 nm) and the vibrational frequency is 2,850 cm^{-1}, which means that the Stokes and CARS wavelengths are 1,036 nm and 651 nm, respectively. For simplicity, in FL, we assume that the fluorescence wavelength is the same as the excitation wavelength.

Next, we consider the OTFs of SRL and CARS microscopy. In the previous section, we defined the OTFs of the real and imaginary parts of $\chi^{(3)}$ as $\mathrm{OTF_r}(\boldsymbol{f}) = iA(\boldsymbol{f}) - iA^*(-\boldsymbol{f})$ and $\mathrm{OTF_i}(\boldsymbol{f}) = -A(\boldsymbol{f}) - A^*(-\boldsymbol{f})$, respectively. This holds true for SRL because the local oscillator is the pump beam itself, which causes a Gouy phase shift of $-i$ in the vicinity of the focus of the excitation beam in the sample. In CARS, however, the non-resonant background, whose $\chi^{(3)}$ is a positive real number, acts as the local oscillator. The constant before the local oscillator becomes unity in CARS because the non-resonant background is generated from the sample with an initial phase of zero. Here, the non-resonant background is assumed to be spectrally flat and have homogeneous intensity over the sample. In this case, the OTF of CARS microscopy changes as follows: $\mathrm{OTF_r}(\boldsymbol{f}) = A(\boldsymbol{f}) + A^*(-\boldsymbol{f})$ and $\mathrm{OTF_i}(\boldsymbol{f}) = iA(\boldsymbol{f}) - iA^*(-\boldsymbol{f})$. If $A(\boldsymbol{f}) = A^*(-\boldsymbol{f})$, $\mathrm{OTF_r}(\boldsymbol{f})$ in SRL and $\mathrm{OTF_i}(\boldsymbol{f})$ in CARS vanish, but if $A(\boldsymbol{f}) \neq A^*(-\boldsymbol{f})$, they remain. Consequently, in SRL under the condition $A(\boldsymbol{f}) \neq A^*(-\boldsymbol{f})$, the real part of $\chi^{(3)}$, which also contains cross phase modulation (XPM, an optical process), appears in the image. Similarly, in CARS under the condition $A(\boldsymbol{f}) \neq A^*(-\boldsymbol{f})$, the imaginary part of $\chi^{(3)}$ is observed.

We now consider nonconfocal microscopy, which is normally used to obtain a high signal intensity. Although in nonconfocal microscopy the detector is normally placed at the plane conjugate to the pupil of the collection objective, we consider the microscopy in which the detector is placed at the image plane conjugate to the sample plane. Note that, in nonconfocal microscopy, the image does not change regardless of the detector position. Therefore, to simplify the equation, we calculate the intensity value at a certain sample-stage displacement (x', y', z') by three-dimensionally integrating the signal intensity in the detection space. The image intensity acquired by nonconfocal microscopy is proportional to [16)20)]

$$
\begin{aligned}
I(\boldsymbol{x}') &\propto \iiint \left| cE_{\mathrm{lo}}(\boldsymbol{x}_{\mathrm{d}}) + \iiint \chi^{(3)}_{\mathrm{CRS}}(\boldsymbol{x}-\boldsymbol{x}')\left[E^3_{\mathrm{ex}}(\boldsymbol{x})\right] h_{\mathrm{col}}(\boldsymbol{x}_{\mathrm{d}}-\boldsymbol{x}) d^3\boldsymbol{x} \right|^2 d^3\boldsymbol{x}_{\mathrm{d}} \\
&\approx \iiint \left| E_{\mathrm{lo}}(\boldsymbol{x}_{\mathrm{d}}) \right|^2 d^3\boldsymbol{x}_{\mathrm{d}} \\
&\quad + c^* E^*_{\mathrm{lo}} \iiint \chi^{(3)}_{\mathrm{CRS}}(\boldsymbol{x}-\boldsymbol{x}')\left[E^3_{\mathrm{ex}}(\boldsymbol{x})\right] h_{\mathrm{col}}(-\boldsymbol{x}) d^3\boldsymbol{x} + c.c., \qquad (14)
\end{aligned}
$$

where $E_{\mathrm{lo}}(\boldsymbol{x}_{\mathrm{d}})$ is the local oscillator, c is $-i$ for SRL and unity for CARS, and $[E^3_{\mathrm{ex}}(\boldsymbol{x})]$ represents the excitation field including the pump and Stokes beams. In Eq. (14), the fourth term was neglected and the relation $\iiint E^*_{\mathrm{lo}}(\boldsymbol{x}_{\mathrm{d}})\, h_{\mathrm{col}}(\boldsymbol{x}_{\mathrm{d}}-\boldsymbol{x}) d^3\boldsymbol{x}_{\mathrm{d}} \approx E^*_{\mathrm{lo}}\, h_{\mathrm{col}}(-\boldsymbol{x})$ was used, assuming that $E_{\mathrm{lo}}(\boldsymbol{x}_{\mathrm{d}}) \approx E_{\mathrm{lo}}\, h_{\mathrm{col}}(\boldsymbol{x}_{\mathrm{d}})$ if $\mathrm{NA_{ex}} \geq \mathrm{NA_{col}}$. The first term in Eq. (14) is a constant, which vanishes with lock-in detection in SRL, and can be eliminated on the computer in CARS. The cross terms (second and third terms) form an image.

We now consider the influence of NA on the OTF in CARS and SRL microscopy. By considering the excitation fields $E_{\mathrm{p}}(\boldsymbol{x})\, E^*_{\mathrm{S}}(\boldsymbol{x})\, E_{\mathrm{p}}(\boldsymbol{x})$ in CARS and $E_{\mathrm{p}}(\boldsymbol{x})\, E^*_{\mathrm{S}}(\boldsymbol{x})\, E_{\mathrm{S}}(\boldsymbol{x})$ in SRL, we analyze the key factor $h_{\mathrm{t}}(-\boldsymbol{x}) = [E^3_{\mathrm{ex}}(\boldsymbol{x})] h_{\mathrm{col}}(-\boldsymbol{x})$ that determines the optical resolution, where $E_{\mathrm{p}}(\boldsymbol{x})$ and $E_{\mathrm{S}}(\boldsymbol{x})$ are the electric field distribution in the sample for the pump and Stokes beams, respectively. Note that $[E^3_{\mathrm{ex}}(\boldsymbol{x})]$ is formed by the excitation system, while $h_{\mathrm{col}}(-\boldsymbol{x})$ is formed by the signal-collection system. In other words, the Fourier transforms of $E_{\mathrm{p}}(\boldsymbol{x})$ and $E_{\mathrm{S}}(\boldsymbol{x})$, i.e., $P_{\mathrm{p}}(\boldsymbol{f})$ and $P_{\mathrm{S}}(\boldsymbol{f})$, are the spherical-shell shaped pupil functions of the excitation system, determined by the wavelength and NA, while $h_{\mathrm{col}}(-\boldsymbol{x})$ is the Fourier transform of the pupil function of the signal-collection system $P_{\mathrm{col}}(\boldsymbol{f})$. Moreover, note that the radius of $P_{\mathrm{col}}(\boldsymbol{f})$ of SRL differs from that of CARS. The 3-D aperture $A(\boldsymbol{f})$, i.e., the Fourier transform of $h_{\mathrm{t}}(-\boldsymbol{x})$, is calculated by convolving the

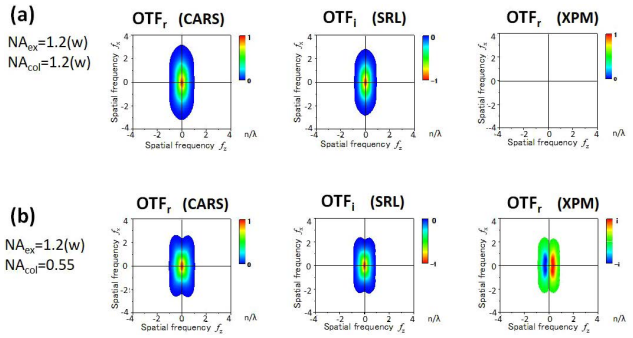

Fig. 6 OTF for CARS, SRL, and XPM. n is the average refractive index in the sample. The wavelengths of the pump and Stokes beams are 800 and 1036 nm, respectively. The vibrational frequency is assumed to be 2850 cm^{-1}. (a) NA_{ex} = 1.2, NA_{col} = 1.2. (b) NA_{ex} = 1.2, NA_{col} = 0.55.

four pupil functions: $P_p(-\boldsymbol{f}) \otimes P_S^*(\boldsymbol{f}) \otimes P_S(-\boldsymbol{f}) \otimes P_{col}(\boldsymbol{f})$ for SRL and $P_p(-\boldsymbol{f}) \otimes P_S^*(\boldsymbol{f}) \otimes P_p(-\boldsymbol{f}) \otimes P_{col}(\boldsymbol{f})$ for CARS. Therefore, if $NA_{ex} \geq NA_{col}$, the 3-D aperture $A(\boldsymbol{f})$ becomes asymmetric, i.e., $A(\boldsymbol{f}) \neq A^*(-\boldsymbol{f})$, resulting in the appearance of XPM in SRL microscopy images. On the other hand, if $NA_{ex} = NA_{col}$ (or even $NA_{ex} \leq NA_{col}$), the XPM disappears from the image. Note that, if the three focal points (excitation system for the pump beam, excitation system for the Stokes beam, and signal-collection system) do not coincide with one another in the sample, XPM emerges even in the case of $NA_{ex} = NA_{col}$.

Fig. 6 shows the NA dependency of the OTF in CARS and SRL microscopy, where we assume that, in SRL microscopy, the wavelengths of the pump and Stokes beams are tuned to a full-resonant vibrational level, and in CARS microscopy, they are slightly detuned to observe $\mathrm{Re}\{\chi^{(3)}_{CARS}\}$. Under the same excitation conditions, CARS microscopy exhibits a slightly higher optical resolution than SRL microscopy owing to the difference in the signal wavelength. In SRL microscopy, if $NA_{ex} \geq NA_{col}$, the OTF of the XPM appears, which is usually undesired. Because the XPM point spread function, calculated by Fourier transforming the OTF, becomes an odd function in the z-direction, the XPM image seems a differential image with respect to z.

10 Conclusion

We have applied the Feynman diagram technique to calculate the laser microscopy resolution limit. This method allows the description of linear, nonlinear, coherent, and incoherent interactions. By performing the calculations, simple rules for the evaluation of 3-D apertures were derived. The 3-D aperture can be calculated by connecting the 3-D pupil functions corresponding to each arrow in a diagram with convolution. Our theory implies that, without *a priori* information on the sample, the type of optical process determines the resolution limit.

11 Appendix

The plane wave of a laser beam can be assumed to be in a coherent state with the frequency $\boldsymbol{f} = (f_x, f_y, f_z)$

$$|\alpha\rangle_{ex} = \prod_{\boldsymbol{f} \in P_{ex}(\boldsymbol{f})} |\alpha\rangle_{\boldsymbol{f}}, \tag{A1}$$

where α is a complex number and $|n\rangle_{\boldsymbol{f}}$ is the number state for the plane wave with frequency $\boldsymbol{f}$ (wavenumber $\boldsymbol{k} = 2\pi\boldsymbol{f}$). Because the excitation laser beam is focused onto the sample by the excitation objective, the corresponding excitation state is represented by the direct product of all modes restricted by the NA and wavelength:

$$|\alpha\rangle_{\boldsymbol{f}} = e^{-\frac{|\alpha|^2}{2}} \sum_{n=0}^{\infty} \frac{\alpha^n}{\sqrt{n!}} |n\rangle_{\boldsymbol{f}}, \tag{A2}$$

where P_{ex} represents the 3-D pupil function for the excitation objective. In coherent optical processes, we consider only the coherent states for laser beams. If two different laser beams (ex1 and ex2) are employed for the excitation, the state representing the excitation condition becomes $|\alpha\rangle_{ex1} |\alpha\rangle_{ex2}$.

For incoherent optical processes, we incorporate the vacuum state $|0\rangle$ into the formulation as one of the excitation lights. For this purpose, we consider the direct product of the coherent state and vacuum state $|\alpha\rangle_{ex}|0\rangle$ as the excitation condition. The vacuum state $|0\rangle$ contains all modes $|0\rangle_{\boldsymbol{f}}$ with frequencies $\boldsymbol{f}$:

$$|0\rangle = \prod_{\boldsymbol{f}} |0\rangle_{\boldsymbol{f}}. \tag{A3}$$

This vacuum state exists around the sample. Note that the contribution of $|0\rangle_{\boldsymbol{f}}$ in $|\alpha\rangle_{\boldsymbol{f}}$ is negligible because of the normal order product for the operator, which will be explained later.

We introduce the basic idea of the annihilation and creation operators in real space, $\hat{a}(\boldsymbol{x})$ and $\hat{a}^+(\boldsymbol{x})$, using the 3-D pupil function $P(\boldsymbol{f})$:

$$\hat{a}(\boldsymbol{x}) = \int P(\boldsymbol{f})\, \hat{a}(\boldsymbol{f}) e^{i2\pi \boldsymbol{f}\cdot\boldsymbol{x}} d^3\boldsymbol{f}, \tag{A4}$$

$$\hat{a}^+(\boldsymbol{x}) = \int P^*(\boldsymbol{f})\, \hat{a}^+(\boldsymbol{f}) e^{-i2\pi \boldsymbol{f}\cdot\boldsymbol{x}} d^3\boldsymbol{f}, \tag{A5}$$

where $\hat{a}(\boldsymbol{f})$ and $\hat{a}^+(\boldsymbol{f})$ are the annihilation and creation operators in the wavenumber domain, respectively. Using this underlying concept, we can define the annihilation operators in real space for the excitation laser field $\hat{a}_{ex}(\boldsymbol{x})$, the vacuum field around the sample $\hat{a}_{vac}(\boldsymbol{x})$, the local oscillator field derived from the vacuum field $\hat{a}_{lo(v)}(\boldsymbol{x})$, the local oscillator field due to the excitation laser field $\hat{a}_{lo(l)}(\boldsymbol{x})$, the

signal field emitted from the sample $\hat{a}_{\mathrm{sig}}(\boldsymbol{x})$, and the signal field collected into the detector $\hat{a}_{\mathrm{col}}(\boldsymbol{x})$ as

$$\begin{aligned}
&\hat{a}_{\mathrm{ex}}(\boldsymbol{x}) = \int P_{\mathrm{ex}}(\boldsymbol{f})\,\hat{a}(\boldsymbol{f}) e^{i2\pi \boldsymbol{f}\cdot\boldsymbol{x}} d^3\boldsymbol{f},\\
&\hat{a}_{\mathrm{vac}}(\boldsymbol{x}) = \int V(\boldsymbol{f})\delta\left(|\boldsymbol{f}| - f_{\mathrm{sig}}\right)\hat{a}(\boldsymbol{f}) e^{i2\pi \boldsymbol{f}\cdot\boldsymbol{x}} d^3\boldsymbol{f},\\
&\hat{a}_{\mathrm{lo(v)}}(\boldsymbol{x}_{\mathrm{d}}) = \int V(\boldsymbol{f}_{\mathrm{d}}) P_{\mathrm{col}}(\boldsymbol{f}_{\mathrm{d}})\,\hat{a}(\boldsymbol{f}_{\mathrm{d}}) e^{i2\pi \boldsymbol{f}_{\mathrm{d}}\cdot\boldsymbol{x}_{\mathrm{d}}} d^3\boldsymbol{f}_{\mathrm{d}},\\
&\hat{a}_{\mathrm{lo(l)}}(\boldsymbol{x}_{\mathrm{d}}) = \int P_{\mathrm{ex}}(\boldsymbol{f}_{\mathrm{d}}) P_{\mathrm{col}}(\boldsymbol{f}_{\mathrm{d}})\,\hat{a}(\boldsymbol{f}_{\mathrm{d}}) e^{i2\pi \boldsymbol{f}_{\mathrm{d}}\cdot\boldsymbol{x}_{\mathrm{d}}} d^3\boldsymbol{f}_{\mathrm{d}},\\
&\hat{a}_{\mathrm{sig}}(\boldsymbol{x}) = \int \delta_{+}\left(|\boldsymbol{f}| - f_{\mathrm{sig}}\right)\hat{a}(\boldsymbol{f}) e^{i2\pi \boldsymbol{f}\cdot\boldsymbol{x}} d^3\boldsymbol{f},\\
&\hat{a}_{\mathrm{col}}(\boldsymbol{x}_{\mathrm{d}}) = \int P_{\mathrm{col}}(\boldsymbol{f}_{\mathrm{d}})\,\hat{a}(\boldsymbol{f}_{\mathrm{d}}) e^{i2\pi \boldsymbol{f}_{\mathrm{d}}\cdot\boldsymbol{x}_{\mathrm{d}}} d^3\boldsymbol{f}_{\mathrm{d}},
\end{aligned} \tag{A6}$$

with

$$\begin{aligned}
&P_{\mathrm{ex}}(f_x, f_y, f_z) = P_{\mathrm{ex}}^{(2)}(f_x, f_y) P_{\mathrm{ex}}^{(3)}(f_x, f_y, f_z),\\
&\delta_{+}\left(|\boldsymbol{f}| - f_{\mathrm{sig}}\right) = \delta\left(|\boldsymbol{f}| - f_{\mathrm{sig}}\right) + \frac{1}{i\pi\left(|\boldsymbol{f}| - f_{\mathrm{sig}}\right)},
\end{aligned} \tag{A7}$$

where $P_{\mathrm{ex}}(\boldsymbol{f})$ is the 3-D pupil function for the excitation system expressed by the product of the 2-D pupil function for the excitation system $P_{\mathrm{ex}}^{(2)}(f_{\mathrm{x}}, f_{\mathrm{y}})$ (including laser beam profile) and the spherical shell truncated by *NA* $P_{\mathrm{ex}}^{(3)}(f_{\mathrm{x}}, f_{\mathrm{y}}, f_{\mathrm{z}})$, which has delta-function characteristics in the radial direction. $V(\boldsymbol{f})$ represents the complex random function whose modulus is one, $P_{\mathrm{col}}(\boldsymbol{f})$ is the 3-D pupil function for the signal-collection system, which is the partial sphere with the modulus of one, and f_{sig} is the modulus of the wavenumber for the signal field. Note that f_{sig} takes into account the refractive index of the sample. The information on the aberration is included in the pupil functions.

We now establish the operators ordering. The operators $\hat{a}_{\mathrm{ex}}(\boldsymbol{x})$ and $\hat{a}_{\mathrm{lo(l)}}(\boldsymbol{x}_{\mathrm{d}})$ act on $|\alpha\rangle_{\mathrm{ex}}$, and the operators $\hat{a}_{\mathrm{vac}}(\boldsymbol{x})$, $\hat{a}_{\mathrm{lo(v)}}(\boldsymbol{x}_{\mathrm{d}})$, $\hat{a}_{\mathrm{sig}}(\boldsymbol{x})$, and $\hat{a}_{\mathrm{col}}(\boldsymbol{x}_{\mathrm{d}})$ act on $|0\rangle$. For the operator ordering, we introduce the symbol ⋮ ⋮. In the area between the symbols ⋮ ⋮, the order of the operators is rearranged as follows:

- Rule for the operators acting on $|\alpha\rangle_{\mathrm{ex}}$
  Normal ordered product: creation operators are placed to the left of the annihilation operators in the product.
- Rule for the operators acting on $|0\rangle$
  Anti-normal ordered product: annihilation operators are placed to the left of creation operators in the product.

The special ordered product defined above means that the vacuum field cannot be observed, except when considering the propagator represented as the vacuum expectation value, such as $\langle 0|\,\hat{a}_{\mathrm{col}}(\boldsymbol{x}_{\mathrm{d}})\,\hat{a}^{+}_{\mathrm{sig}}(\boldsymbol{x})\,|0\rangle$. Note that we ignore the vacuum expectation value $\langle 0|\,\hat{a}_{\mathrm{lo(v)}}(\boldsymbol{x}_{\mathrm{d}})\,\hat{a}^{+}_{\mathrm{lo(v)}}(\boldsymbol{x}_{\mathrm{d}})\,|0\rangle$, which cannot be observed in practical experiments.

To unify the framework for coherent and incoherent optical processes, the classical field is replaced by the operator. Then, the operator acts on the bra or ket describing the excitation condition. Because the vacuum field inevitably exists around the sample, we always utilize both the coherent state for the laser and the vacuum state as the excitation condition, such as $|\alpha\rangle_{\mathrm{ex}}\,|0\rangle$. For example, using the relation $\hat{a}_{\mathrm{ex}}(\boldsymbol{f})|\alpha\rangle_{f} = \alpha\,|\alpha\rangle_{f}$, the calculation is as follows:

$$\begin{aligned}
\hat{a}_{\mathrm{ex}}(\boldsymbol{x})|\alpha\rangle_{\mathrm{ex}} &= \int P_{\mathrm{ex}}(\boldsymbol{f})\,\hat{a}(\boldsymbol{f}) e^{i2\pi \boldsymbol{f}\cdot\boldsymbol{x}} d^3\boldsymbol{f}\,|\alpha\rangle_{\mathrm{ex}}\\
&= \int P_{\mathrm{ex}}(\boldsymbol{f})\,\alpha\, e^{i2\pi \boldsymbol{f}\cdot\boldsymbol{x}} d^3\boldsymbol{f}\,|\alpha\rangle_{\mathrm{ex}}\\
&= \alpha\, ASF_{\mathrm{ex}}(\boldsymbol{x})|\alpha\rangle_{\mathrm{ex}},
\end{aligned} \tag{A8}$$

where $ASF_{\mathrm{ex}}(\boldsymbol{x})$ is the ASF formed by the excitation laser beam onto the sample through the excitation objective. The calculation related to the vacuum field is as follows:

$$\begin{aligned}
\langle 0|\hat{a}_{\mathrm{col}}(\boldsymbol{x}_{\mathrm{d}})\hat{a}^{\dagger}_{\mathrm{sig}}(\boldsymbol{x})|0\rangle &= \int P_{\mathrm{col}}(\boldsymbol{f})\delta^{*}_{+}\left(|\boldsymbol{f}| - f_{\mathrm{sig}}\right) e^{i2\pi \boldsymbol{f}\cdot(\boldsymbol{x}_{\mathrm{d}} - \boldsymbol{x})} d^3\boldsymbol{f}\\
&= ASF_{\mathrm{col}}(\boldsymbol{x}_{\mathrm{d}} - \boldsymbol{x}),
\end{aligned} \tag{A9}$$

$$\begin{aligned}
\langle 0|\hat{a}_{\mathrm{vac}}(\boldsymbol{x})\hat{a}^{\dagger}_{\mathrm{lo(v)}}(\boldsymbol{x}_{\mathrm{d}})|0\rangle &= \left\{\int |V(\boldsymbol{f})|^2 P_{\mathrm{col}}(\boldsymbol{f})\delta\left(|\boldsymbol{f}| - f_{\mathrm{sig}}\right) e^{i2\pi \boldsymbol{f}\cdot(\boldsymbol{x}_{\mathrm{d}} - \boldsymbol{x})} d^3\boldsymbol{f}\right\}^{*}\\
&= \left\{ASF_{\mathrm{col}}(\boldsymbol{x}_{\mathrm{d}} - \boldsymbol{x})\right\}^{*},
\end{aligned} \tag{A10}$$

$$\begin{aligned}
\langle 0|\hat{a}_{\mathrm{sig}}(\boldsymbol{x})\hat{a}^{\dagger}_{\mathrm{col}}(\boldsymbol{x}_{\mathrm{d}})|0\rangle &= \left\{\langle 0|\hat{a}_{\mathrm{col}}(\boldsymbol{x}_{\mathrm{d}})\hat{a}^{\dagger}_{\mathrm{sig}}(\boldsymbol{x})|0\rangle\right\}^{*}\\
&= \left\{ASF_{\mathrm{col}}(\boldsymbol{x}_{\mathrm{d}} - \boldsymbol{x})\right\}^{*},
\end{aligned} \tag{A11}$$

where $ASF_{\mathrm{col}}(\boldsymbol{x}_{\mathrm{d}})$ is the ASF formed by the signal field onto the detector through the signal-collection objective. Eq. (A9) represents the propagator for the photon that is created at $\boldsymbol{x}$ and annihilated at $\boldsymbol{x}_{\mathrm{d}}$. In Eqs. (A10) and (A11), the left-hand side, which appears to be the light propagation from $\boldsymbol{x}_{\mathrm{d}}$ to $\boldsymbol{x}$, physically indicates that the light expressed by the complex conjugate propagates from $\boldsymbol{x}$ to $\boldsymbol{x}_{\mathrm{d}}$.

For the convenience of formulas transformation and simplification, we calculate the commutation relation between the annihilation and creation operators in real space:

$$\begin{aligned}
&\left[\hat{a}_{\mathrm{col}}(\boldsymbol{x}_{\mathrm{d}}), \hat{a}^{\dagger}_{\mathrm{col}}(\boldsymbol{x}_{\mathrm{d}})\right]\\
&= \hat{a}_{\mathrm{col}}(\boldsymbol{x}_{\mathrm{d}})\hat{a}^{\dagger}_{\mathrm{col}}(\boldsymbol{x}_{\mathrm{d}}) - \hat{a}^{\dagger}_{\mathrm{col}}(\boldsymbol{x}_{\mathrm{d}})\hat{a}_{\mathrm{col}}(\boldsymbol{x}_{\mathrm{d}})\\
&= \int P_{\mathrm{col}}(\boldsymbol{f}_1)\,\hat{a}(\boldsymbol{f}_1) e^{i2\pi \boldsymbol{f}_1\cdot\boldsymbol{x}_{\mathrm{d}}} d^3\boldsymbol{f}_1 \int P^{*}_{\mathrm{col}}(\boldsymbol{f}_2)\,\hat{a}^{+}(\boldsymbol{f}_2) e^{-i2\pi \boldsymbol{f}_2\cdot\boldsymbol{x}_{\mathrm{d}}} d^3\boldsymbol{f}_2\\
&\quad - \int P^{*}_{\mathrm{col}}(\boldsymbol{f}_2)\,\hat{a}^{+}(\boldsymbol{f}_2) e^{-i2\pi \boldsymbol{f}_2\cdot\boldsymbol{x}_{\mathrm{d}}} d^3\boldsymbol{f}_2 \int P_{\mathrm{col}}(\boldsymbol{f}_1)\,\hat{a}(\boldsymbol{f}_1) e^{i2\pi \boldsymbol{f}_1\cdot\boldsymbol{x}_{\mathrm{d}}} d^3\boldsymbol{f}_1\\
&= \iint P_{\mathrm{col}}(\boldsymbol{f}_1) P^{*}_{\mathrm{col}}(\boldsymbol{f}_2)\left\{\hat{a}(\boldsymbol{f}_1)\hat{a}^{+}(\boldsymbol{f}_2) - \hat{a}^{+}(\boldsymbol{f}_2)\hat{a}(\boldsymbol{f}_1)\right\} e^{i2\pi(\boldsymbol{f}_1 - \boldsymbol{f}_2)\cdot\boldsymbol{x}_{\mathrm{d}}} d^3\boldsymbol{f}_1 d^3\boldsymbol{f}_2\\
&= \iint P_{\mathrm{col}}(\boldsymbol{f}_1) P^{*}_{\mathrm{col}}(\boldsymbol{f}_2)\left[\hat{a}(\boldsymbol{f}_1), \hat{a}^{+}(\boldsymbol{f}_2)\right] e^{i2\pi(\boldsymbol{f}_1 - \boldsymbol{f}_2)\cdot\boldsymbol{x}_{\mathrm{d}}} d^3\boldsymbol{f}_1 d^3\boldsymbol{f}_2\\
&= \iint P_{\mathrm{col}}(\boldsymbol{f}_1) P^{*}_{\mathrm{col}}(\boldsymbol{f}_2)\delta(\boldsymbol{f}_1 - \boldsymbol{f}_2) e^{i2\pi(\boldsymbol{f}_1 - \boldsymbol{f}_2)\cdot\boldsymbol{x}_{\mathrm{d}}} d^3\boldsymbol{f}_1 d^3\boldsymbol{f}_2\\
&= \int |P_{\mathrm{col}}(\boldsymbol{f})|^2 d^3\boldsymbol{f},
\end{aligned} \tag{A12}$$

where the commutation relation in frequency domain $[\hat{a}(\boldsymbol{f}_1), \hat{a}^{+}(\boldsymbol{f}_2)] = \delta(\boldsymbol{f}_1 - \boldsymbol{f}_2)$ is used. Likewise, we obtain

$$\begin{aligned}
\left[\hat{a}_{\mathrm{col}}(\boldsymbol{x}_{\mathrm{d}}), \hat{a}^{+}_{\mathrm{lo(v)}}(\boldsymbol{x}_{\mathrm{d}})\right] &= \int V^{*}(\boldsymbol{f}_{\mathrm{d}})\left|P_{\mathrm{col}}(\boldsymbol{f}_{\mathrm{d}})\right|^2 d^3\boldsymbol{f}_{\mathrm{d}}\\
&= 0,
\end{aligned} \tag{A13}$$

where the random phase nature of $V^{*}(\boldsymbol{f}_{\mathrm{d}})$ is used.

References

1) E. Abbe: *Archiv für Mikroskopische Anatomie* (in German). Bonn Germany, Verlag von Max Cohen & Sohn **9** (1), 413–468 (1873).
2) A. Köhler: *Zeitschrift für wissenschaftliche Mikroskopie und*

für Mikroskopische Technik, **10** (4), 433–440 (1893).
3) F. Zernike: *Physica*, **9** (7), 686–698 (1942).
4) F. Zernike: *Physica*, **9** (10), 974–986 (1942).
5) G. Nomarski: *J. Phys. Radium*, **16**, 9 (1955).
6) R. Zsigmondy: *John Wiley & Sons,* 1st ed. (1914).
7) R. Hoffman and L. Gross: *Applied Optics Microscope*, **14**, 1169–1176 (1975).
8) T. Zhang and I. Yamaguchi: *Optics Letters*, **23** (15), 1221–1223 (1998).
9) D. Huang, E. A. Swanson, C. P. Lin, J. S. Schuman, W. G. Stinson, W. Chang, M. R. Hee, T. Flotte, K. Gregory, C. A. Puliafito and J. G. Fujimoto: *Science*, **254**, 1178–1181 (1991).
10) W. Denk, J. H. Strickler and W. W. Webb: *Science*, **248**, 73–76 (1990).
11) I. Freund and M. Deutsch: *Opt. Lett.*, **11**, 94–96 (1986).
12) Y. Barad, H. Eisenberg, M. Horowitz and Y. Silberberg: *Appl. Phys. Lett.*, **70**, 922–924 (1997).
13) A. Zumbusch, G. R. Holtom and X. S. Xie: *Phys. Rev. Lett.*, **82**, 4142–4145 (1999).
14) W. Freudiger, W. Min, B. G. Saar, S. Lu, G. R. Holtom, C. He, J. C. Tsai, J. X. Kang and X. S. Xie: *Science*, **322**, 1857–1861 (2008).
15) C. J. R. Sheppard and C. J. Cogswell: *Journal of Microscopy*, **159** (2), 179–194 (1990).
16) N. Fukutake: *J. Opt. Soc. Am. B*, **30**, 2665–2675 (2013).
17) T. K. Yee and T. K. Gustafson: *Phys. Rev. A*, **18**, 1597 (1978).
18) S. Mukamel: [*Principle of Nonlinear Optical Spectroscopy*], Oxford University Press, New York, (1995).
19) C. J. R. Sheppard and X. Q. Mao: *J. Opt. Soc. Am. A*, **6**, 1260–1269 (1989).
20) N. Fukutake: [*MICROSCOPY AND ANALYSIS*], INTECH (Chapter 1), Rijeka (Croatia), (2016).
21) N. Fukutake: *SPIE proceedings*, 10500 (2018).